Numerical Modeling of Enhanced Nitrogen Dissolution during Gas Tungsten Arc Welding

T.A. PALMER and T. DEBROY

Weld-metal nitrogen concentrations far in excess of Sieverts-law calculations during gas tungsten arc (GTA) welding of iron are investigated both experimentally and theoretically. A transient, three-dimensional mathematical model has been developed to calculate the residual nitrogen concentrations during GTA welding. This model combines calculations for the plasma phase with those for nitrogen absorption and for the transport of nitrogen by convection and diffusion in the weld metal and diffusion throughout the weldment. In addition, the model takes into account the roles of turbulence and the nitrogen desorption reaction in affecting the residual nitrogen concentration in the weldment. Autogeneous GTA welding experiments in pure iron have been performed and the resulting nitrogen concentrations compared with the modeling results. Both experimental and modeled nitrogen concentrations fall in a range between 2.7 and 4.7 times higher than Sieverts-law calculations at a temperature of 2000 K. Modeled nitrogen concentrations correlate well with the experimental results, both in magnitude and in the general trends, with changes in the travel speed and nitrogen addition to the shielding gas.

I. INTRODUCTION

CONCENTRATIONS of diatomic gases, such as hydrogen, oxygen, and nitrogen, are observed in the weld metal during arc welding processes at levels far in excess of Sieverts-law calculations. In particular, nitrogen contents as high as 0.2 wt pct have been obtained in steel welds during arc welding.[1–9] Nitrogen in the weld metal can originate from a variety of sources, depending on the welding operation in question. For example, nitrogen in the weld metal can originate from the interaction between the surrounding atmosphere, which is about 80 pct nitrogen, and the plasma phase above the weld-pool. Impingement of the surrounding atmosphere into the arc column can be due, in part, to insufficient shielding of the weld metal.

Several researchers[2–8] have provided experimental results of gas tungsten arc (GTA) welding experiments in nitrogen-containing atmospheres for a variety of base-metal compositions. Results for the GTA welding of iron in nitrogen-containing atmospheres is shown in Figure 1. In this figure, the weld-metal nitrogen concentration is plotted as a function of the nitrogen partial pressure in the shielding gas and is compared with Sieverts-law calculations for three temperatures in liquid iron.[7] The observed nitrogen concentrations in the weld metal are significantly higher than Sieverts-law calculations. Nitrogen concentrations in the weld-pool at these levels are considered to be the result of the interaction between a nitrogen-containing plasma phase and liquid iron.

The mechanisms responsible for these enhanced nitrogen concentrations in an iron weld-pool have been of significant interest. In both arc melting and arc welding operations, a plasma phase exists above the liquid metal. This plasma phase, which is composed of a number of different species not normally observed in gas-metal systems, significantly alters the nitrogen absorption reaction in liquid iron and steel.[9–17] Monatomic nitrogen (N), which is one such species produced in the plasma phase, is considered to be the species responsible for the observed enhancements in the nitrogen concentration. This role for monatomic nitrogen is based on its significantly higher solubility in iron, with partial pressures many orders of magnitude less than that for diatomic nitrogen.[4,18,19]

Several authors have also proposed that the total amount of nitrogen present in the liquid metal is the balance of two independent processes.[12,20–23] Monatomic nitrogen is absorbed through the interface between the arc and the liquid metal. Once a saturation level is reached at any location on the metal surface, nitrogen is then expelled from the surface of the liquid metal. This expulsion of nitrogen from the weld-pool surface occurs *via* a desorption reaction, in which bubbles form at the surface and other heterogeneous nucleation sites in the liquid melt. These bubbles are filled with nitrogen gas, which has been rejected from the liquid iron. Outside the arc column, the nitrogen in solution in the iron is in equilibrium with diatomic nitrogen rather than monatomic nitrogen, which dominates the arc column.

Models based on the role of the plasma phase in producing these enhanced nitrogen concentrations have also been developed. For example, Gedeon and Eagar[24] have proposed that the diatomic gas introduced into the plasma phase in the arc column partially dissociates at a temperature higher than that at the sample surface. The monatomic species is then transported to the liquid-metal surface, where it is absorbed at the temperature on the liquid-metal surface. Mundra and DebRoy[18] have used this same methodology to develop a semiquantitative model to describe the temperature at which the diatomic gas dissociates in the plasma phase. In these models,[18,24] a hypothetical dissociation temperature (T_d), equal to the temperature at which the equilibrium thermal dissociation of diatomic nitrogen produces the

T.A. PALMER, formerly Graduate Research Assistant with the Department of Materials Science and Engineering, The Pennsylvania State University, is Postdoc with Lawrence Livermore National Laboratory, Livermore, CA 94551. T. DEBROY, Professor, is with the Department of Materials Science and Engineering, The Pennsylvania State University, University Park, PA 16802.

Manuscript submitted December 7, 1999.

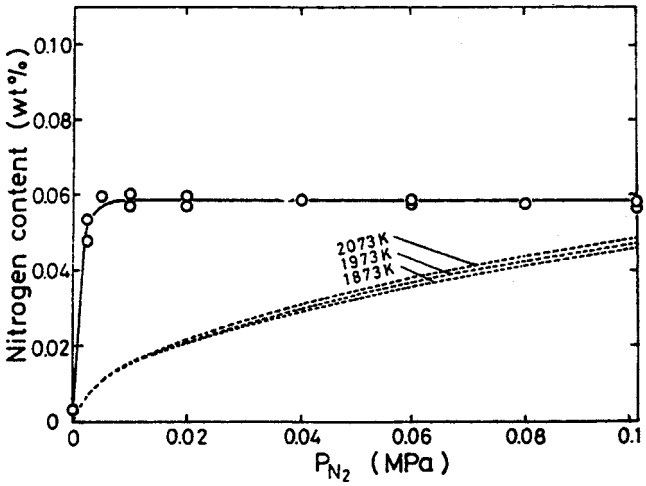

Fig. 1—Relation between the nitrogen content of the weld metal and the nitrogen partial pressure (P_{N_2}) for an Ar-N_2 shielding gas mixture at a welding current of 250 A, an arc length of 0.010 m, and a travel speed of 0.00167 m/s.[7]

partial pressure of monatomic nitrogen in the plasma, is defined. This dissociation temperature is in a range of 100 to 300 K higher than the temperature at the metal surface (T_s) and is a measure of the partial pressure of the atomic nitrogen in the plasma. This methodology, which is termed the two-temperature model, provides an order-of-magnitude agreement between the calculated and experimental nitrogen concentrations.

In the two-temperature model, the dissociation temperature is an adjustable parameter. Therefore, it does not strictly provide a capability for predicting the nitrogen concentration. No quantitative means for predicting the nitrogen concentration in the weld metal currently exists. In developing a quantitative model, it must be recognized that nitrogen dissolution into the weld-pool is intimately tied to several simultaneously occurring physical processes. These processes include the formation of various nitrogen species in the plasma phase above the weld-pool, the nature of reactions at the interface between the plasma phase and the weld-pool surface, and the transport of nitrogen within the weldment by convection and diffusion. A mathematical model, which combines calculations describing each of these processes into a single model, has been developed here. The validity of this model has also been tested by comparing the modeling results with those from a series of GTA welding experiments with pure iron.

II. MODEL DEVELOPMENT

A. *Plasma Phase Calculations*

During GTA welding, the interaction between the tungsten electrode and the inert shielding gas produces a plasma phase above the weld-pool. This plasma phase is characterized by electron temperatures between 3000 and 20,000 K and consists of a number of different ionized and neutral species, depending on the nature of the shielding gas mixture. In the GTA welding of pure iron samples performed here, Ar-N_2 gas mixtures of various compositions have been used. In order to calculate the resulting nitrogen concentration in the weld metal, the partial pressure of monatomic nitrogen above the weld-pool must be known. This value can be determined by calculating the species density of each species present in the plasma phase above the weld-pool as a function of the electron temperatures and the system pressure.

A methodology to calculate the number densities of species present in the plasma phase for a variety of pure gases and gas mixtures was presented in a previous study.[19] This methodology is based on the assumption of local thermodynamic equilibrium (LTE) in the plasma phase. Under LTE conditions, both quasineutrality and an ideal gas-law behavior are assumed to be dominant in the system. In this study, a number of Ar-N_2 gas mixtures have been analyzed, and the species densities of the individual components have been calculated.

In these argon-nitrogen gas mixtures, there are a number of species to be considered, including Ar, Ar^+, Ar^{++}, N_2, N_2^+, and N^+. The ionization reactions for both Ar and N_2 species are shown as follows, along with the accompanying Saha–Eggert relation:[25,26,27]

$$\mathrm{Ar} \rightarrow \mathrm{Ar}^+ + e^- \qquad [1]$$

$$\frac{n_e n_{\mathrm{Ar}^+}}{n_{\mathrm{Ar}}} = \frac{2(2\pi m_e \mathrm{k}T)^{3/2} Z_{\mathrm{Ar}^+}}{h^3 \quad Z_{\mathrm{Ar}}} e^{-(\varepsilon_{\mathrm{Ar}})/\mathrm{k}T} \qquad [2]$$

$$\mathrm{Ar}^+ \rightarrow \mathrm{Ar}^{++} + e^- \qquad [3]$$

$$\frac{n_e n_{\mathrm{Ar}^{++}}}{n_{\mathrm{Ar}^+}} = \frac{2(2\pi m_e \mathrm{k}T)^{3/2}}{h^3} \frac{Z_{\mathrm{Ar}^{++}}}{Z_{\mathrm{Ar}^+}} e^{-(\varepsilon_{\mathrm{Ar}^+})/\mathrm{k}T} \qquad [4]$$

$$\mathrm{N}_2 \rightarrow \mathrm{N}_2^+ + e^- \qquad [5]$$

$$\frac{n_e n_{\mathrm{N}_2^+}}{n_{\mathrm{N}_2}} = \frac{2(2\pi m_e \mathrm{k}T)^{3/2}}{h^3} \frac{Z_{\mathrm{N}_2^+}}{Z_{\mathrm{N}_2}} e^{-(\varepsilon_{\mathrm{N}_2})/\mathrm{k}T} \qquad [6]$$

$$\mathrm{N} \rightarrow \mathrm{N}^+ + e^- \qquad [7]$$

$$\frac{n_e n_{\mathrm{N}^+}}{n_{\mathrm{N}}} = \frac{2(2\pi m_e \mathrm{k}T)^{3/2}}{h^3} \frac{Z_{\mathrm{N}^+}}{Z_{\mathrm{N}}} e^{-(\varepsilon_{\mathrm{N}})/\mathrm{k}T} \qquad [8]$$

where n_e is the electron density, n_i is the number density for each of the respective gaseous species, m_e is the rest mass of an electron, k is the Boltzmann constant (1.38×10^{-23} J K^{-1}), T is the electron temperature (in Kelvin), h is the Planck's constant (6.63×10^{-34} J s), Z_i is the partition function for each gaseous species, and ε_i is the ground-state energy for the species of interest. The partition functions[25–28] are based on the various energy levels of each atomic or molecular species and provide insight into the fundamental nature of the species of interest. Values of the partition functions, which vary with the electron temperature, are calculated elsewhere.[19]

In addition to the ionization reactions occurring in the plasma phase, the dissociation of the diatomic molecules into atomic species is also considered. The dissociation of diatomic nitrogen is given by Eq. [9], and its equilibrium constant (K) is expressed by Eq. [10]:

$$\mathrm{N}_2(\mathrm{g}) \rightarrow 2\mathrm{N}(\mathrm{g}) \qquad [9]$$

$$K = \frac{p_{\mathrm{N}}^2}{p_{\mathrm{N}_2}} = \frac{(P)^2 (X_{\mathrm{N}})^2}{(P) X_{\mathrm{N}_2}} = P \frac{(X_{\mathrm{N}})^2}{X_{\mathrm{N}_2}} = \frac{(n_{\mathrm{N}})^2}{n_{\mathrm{N}_2}} \left(\frac{\mathrm{R}T}{N_{\mathrm{A}}} \right) \qquad [10]$$

where P is the total system pressure (in atmospheres); p_{N} is the partial pressure of monatomic nitrogen; p_{N_2} is the partial pressure of diatomic nitrogen; X_{N} and X_{N_2} are the mole fractions of N and N_2, respectively; n_{N} and n_{N_2} are the

number densities (in m^{-3}) for N and N_2, respectively; R is the gas constant (8.314 J mol^{-1} K^{-1}); and N_A is Avogadro's number (6.022×10^{24} mol^{-1}). At temperatures commonly used for conventional materials processing, the free-energy values are available and the value of K can be easily calculated. On the other hand, accurate thermodynamic data are not readily available for the high temperatures commonly found in the welding plasma. A recourse is to calculate the necessary data, which have been presented elsewhere.[19]

In addition to the relations describing the prevalent reactions in the plasma phase, both the charge and mass of the system must be balanced. The charge balance, which is based on the principle of quasi neutrality in the plasma phase, is shown in Eq. [11]. This reaction is the sum of electrons produced by the ionization reactions. The conservation of mass in the system, which is expressed in Eqs. [12] and [13], is based on the total number of species present in the system being equivalent to the species assumed to be present in the plasma phase.

$$n_e = n_{Ar^+} + 2n_{Ar^{++}} n_{N_2^+} + n_{N^+} \quad [11]$$

$$X_{Ar}\left(N_A\left(\frac{p}{RT}\right)\right) = X_{Ar}(n_{Ar} + 2n_{Ar^+} + 3n_{Ar^{++}}) \quad [12]$$

$$X_{N_2}\left(N_A\left(\frac{p}{RT}\right)\right) = X_{N_2}(n_{N_2} + 2n_{N_2^+} + n_N + 2n_{N^+}) \quad [13]$$

where X_{Ar} and X_{N_2} are the mole fractions of argon and nitrogen, respectively. Equations [2], [4], [6], [8], and [10] through [13] are then solved simultaneously to obtain values for n_{Ar}, n_{Ar^+}, $n_{Ar^{++}}$, n_{N_2}, $n_{N_2^+}$, n_N, n_{N^+}, and n_e, which represent each species considered to exist in the plasma phase at each electron temperature.

B. *Nitrogen Absorption at the Weld-Metal Surface*

Nitrogen is introduced into the weldment only at the top surface. The reaction governing the nitrogen absorption reaction, thus, depends on the location on the weldment surface. In the area underneath the arc column and defined by the liquid weld-pool, the absorption of monatomic nitrogen (N (g) $\rightarrow$ [N] (ppm)) is dominant. The relation used to solve for the nitrogen concentration absorbed on the weld-pool surface is shown subsequently:

$$[\underline{N}] = P_N \, e^{\left(-\frac{\Delta G^\circ_{N_2}}{RT}\right)} \quad [14]$$

where [N] is the nitrogen concentration, P_N is the monatomic nitrogen partial pressure, $\Delta G^\circ_{N(g)}$ is the free-energy relationship for the absorption of monatomic nitrogen, T is the temperature, and R is the gas constant.[10,11,29–31] Table I lists the free-energy relationships for the nitrogen absorption reactions. The monatomic nitrogen partial pressure used here is defined by the electron-temperature distribution above the weld-pool and is calculated using the methodology described previously.

In the region outside the arc column and above the solid portion of the weldment, the nitrogen dissociation reaction is minimal, and the absorption of diatomic nitrogen species (1/2 N_2 (g) $\rightarrow$ [N] (ppm)) in solid iron is predominant. The relation used to solve for the nitrogen concentration due to the absorption of diatomic nitrogen is shown in the following relation:

$$[\underline{N}] = (P_{N_2})^{1/2} \, e^{\left(-\frac{\Delta G^\circ_{N_2}}{RT}\right)} \quad [15]$$

where P_{N_2} is the diatomic nitrogen partial pressure (in megapascals) and $\Delta G^\circ_{N_2}$ (in J/mol) is the free-energy relationship for the absorption of diatomic nitrogen, which is shown in Table I. In this region, the diatomic nitrogen partial pressure outside the arc column is determined using the relation for the thermal dissociation of the diatomic nitrogen at the temperature on the weld-pool surface, whose free-energy relationship is also defined in Table I.

As previous researchers have noted, the residual nitrogen concentration in the weld-pool is governed by a balance between both the nitrogen absorption and desorption reactions. Therefore, the nitrogen desorption reaction is also considered here. In order for nitrogen to leave the weld metal, a certain level of nitrogen concentration in the liquid metal must be reached. Above these nitrogen concentration levels, nitrogen leaves the weld metal. Nitrogen concentrations are, therefore, not allowed to exceed this level, thus controlling the onset of nitrogen desorption.

C. *Nitrogen Transport in the Weldment*

1. *Governing equations*

The absorption of nitrogen on the weld-pool surface and the transport of nitrogen in the weld-pool are based on knowledge of the temperature and fluid-flow fields in the weldment. These values are calculated here using a transient, three-dimensional control volume–based computational procedure developed elsewhere.[32,33] In this procedure, the equations for the conservation of mass, momentum, energy, and the nitrogen concentration in the weld-pool are solved. These equations are formulated in a coordinate system (ζ, y, z, and t)[32] in which the heat source and the molten metal under it are fixed in space, and the material enters and leaves the computational domain at the welding velocity.[34,35] Each equation of conservation is defined subsequently. Table II lists the thermophysical properties used in the solution of these governing equations.[36–39]

The conservation of momentum is represented by the following equation:

$$\frac{\partial}{\partial t}(\rho \mathbf{V}) + \nabla \cdot (\rho \mathbf{V}\mathbf{V}) = -\nabla P + \mu \nabla \cdot (\nabla \mathbf{V}) + S + S_{e-p} - \nabla \cdot (\rho \mathbf{U}\mathbf{V}) \quad [16]$$

where t is the time; μ is the viscosity; ρ is the density; P is the effective pressure; S is the source term, which takes into account both the buoyancy (F_b) and electromagnetic forces ($\mathbf{F}_e$); S_{e-p} is the source term, which modifies the momentum equation in the mushy zone; $\mathbf{U}$ is the welding velocity; $\mathbf{V}$ is the convective velocity term; and $\mathbf{V}'$ is the net velocity ($\mathbf{V}' = \mathbf{V} + \mathbf{U}$).

In this equation, the buoyancy, electromagnetic, and surface-tension forces are taken into account in the calculation of the fluid-flow velocities in the weld-pool. A comparison between the relative magnitudes of these forces has been performed elsewhere.[40] According to these calculations, the buoyancy force is negligible, while the surface-tension force

Table I. Summary of Free Energies Used in Nitrogen Absorption Reactions[7,10,11,29,31,32]

Reaction	Phase	Free Energy (J/mol)	Temperature Range (K)	Reference
1/2 N_2 (g) → N (g)	gas	362,318.0 − 65.52 T	273 to 1811	10
N (g) → $\underline{N}$ (wt pct)	liquid	−358,719.4 + 89.56 T	>1811	10, 11, 31
N (g) → $\underline{N}$ (wt pct)	solid-δ	−349,265.3 + 74.01 T	1663 to 1810	10, 29
N (g) → $\underline{N}$ (wt pct)	solid-γ	−353,698.6 + 10.29 T	1185 to 1662	10, 32
N (g) → $\underline{N}$ (wt pct)	solid-α	−349,265.3 + 74.01 T	273 to 1184	10, 31
1/2 N_2 (g) → $\underline{N}$ (wt pct)	liquid	3598.2 + 23.89 T	>1811	10, 31
1/2 N_2 (g) → $\underline{N}$ (wt pct)	solid-δ	13,052.4 + 8.49 T	1663 to 1810	10, 29
1/2 N_2 (g) → $\underline{N}$ (wt pct)	solid-γ	−8619.0 + 37.40 T	1185 to 1662	7, 29
1/2 N_2 (g) → $\underline{N}$ (wt pct)	solid-α	13,052.4 + 8.49 T	273 to 1184	10, 29

Table II. Summary of the Thermophysical Properties Used in the Calculations Described Here[36–38,47]

Material Property	Value	References
Density of liquid metal (kg/m^3)	7200	47
Liquidus temperature (K)	1811	47
Solidus temperatue (K)	1811	47
Viscosity of liquid (kg/m s)	0.60	36
Viscosity enhancement factor	30	—
Thermal conductivity of solid iron (W/m K)	20.9	36
Thermal conductivity of liquid iron (W/m K)	154	—
Specific heat of solid iron (J/kg K)	702.9	47
Specific heat of liquid iron (J/kg K)	807.5	37
Enthalpy of solid iron at melting point (J/kg)	1.05×10^6	37
Enthalpy of liquid iron at melting point (J/kg)	1.32×10^6	37
Temperature coefficient of surface tension (N/m K)	-4.3×10^{-4}	38
Coefficient of thermal expansion (1/K)	1×10^{-5}	36

is approximately 4 times greater than the electromagnetic force. Therefore, fluid flow in the weld-pool is primarily driven by surface tension or the Marangoni stress, which is a result of the temperature variation of the surface tension and the large temperature gradients characteristic of the weld-pool surface.[41,42]

When solving for the conservation of energy during the arc welding process, the total enthalpy (H) is considered, in order to take into account phase changes in the material. The equation for the conservation of energy is given by the following relationship:

$$\frac{\partial}{\partial t}(\rho h) + \nabla \cdot (\rho \mathbf{V} h) = \nabla \cdot \left(\frac{k}{C_p} \nabla h\right) - \nabla \cdot (\rho \mathbf{V} \Delta H) - \nabla \cdot (\rho \mathbf{U} \Delta H) - \nabla \cdot (\rho \mathbf{U} h) - \frac{\partial}{\partial t}(\rho \Delta H) + S \quad [17]$$

where k is the thermal conductivity and S is the source term. The source term accounts for the latent heat of melting and the convective transport of latent heat.

Monatomic nitrogen absorbed on the weld-pool surface is transported to the interior of the weld-pool through both convective and diffusive processes. The conservation of the nitrogen concentration in the weldment is defined by the following relation.[43]

$$\frac{\partial}{\partial t}(\rho C) + \nabla \cdot (\rho \mathbf{V} C) = \nabla \cdot (\rho D \nabla C) - \nabla \cdot (\rho \mathbf{U} C) \quad [18]$$

where C is the nitrogen concentration and D is the nitrogen diffusion coefficient in iron, whose values are summarized,[36,44–47] as a function of temperature ($D = D_0 e^{-E/RT}$), in Table III. The diffusion coefficients for nitrogen in solid iron are several orders of magnitude lower than those for nitrogen in liquid iron. Therefore, the diffusion of nitrogen in the solid portion of the weldment is only considered in the δ-iron phase, since very little, if any, nitrogen diffuses outside this range during the time scale of the welding process.

There are several features of GTA welding which also affect the solution procedure used here. For example, during arc welding, the weld-pool geometry reaches steady-state conditions in a very short time after the start of welding. This condition allows the transient terms from the governing equations to be removed and the steady-state versions of the governing equations for conservation of mass, momentum, and energy to be solved. On the other hand, the nitrogen-concentration calculations are time dependent. Therefore, the governing equations for momentum and energy are solved separately from the equation of conservation of nitrogen concentration. A nonuniform grid ($96 \times 25 \times 26$) has been used to solve all of these equations and to account for the large temperature gradients commonly present in welding operations.

2. *Role of turbulence*

The previous equations are based on the assumption of laminar flow in the weld-pool. On the other hand, fluid flow in weld-pool has been found to be turbulent in nature.[48–50] In several cases, the turbulent flow in the weld-pool has been taken into account by enhancing both the viscosity and thermal conductivity.[32,33,51–53] By enhancing these values, the predicted shape and size of the weld-pool more closely match those observed experimentally. The levels of enhancement to these values have been examined elsewhere,[52] and they tend to be rather empirical in nature. In the calculations presented here, the enhancement to the viscosity is given in Table II.

The use of enhanced viscosity and thermal conductivity values is common in computational fluid dynamics, to take into account turbulent flow.[54] In such calculations, the energy dissipation due to turbulence is taken into account by locally increasing the viscosity. This effective viscosity is the sum of the molecular viscosity, which is a physical property of the fluid, and the turbulent viscosity, which is

Table III. Summary of Nitrogen Diffusion Constants in α, γ, δ, and Liquid Iron Phases[36,47]

Iron Phase	Temperature Range (K)	D (m^2/s)	D_0 (m^2/s)	E (J/mol)	Reference
α	273 to 1184	—	7.80×10^{-7}	7.91×10^{4}	47
γ	1185 to 1662	—	9.10×10^{-5}	1.68×10^{5}	47
δ	1663 to 1810	—	7.80×10^{-7}	7.91×10^{4}	47
Liquid	>1811	1.10×10^{-8}	—	—	36, 47

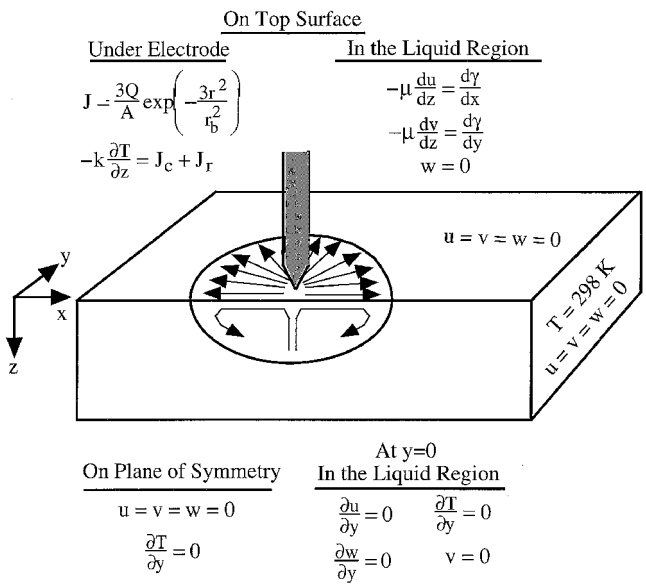

Fig. 2—Summary of boundary conditions used in the mathematical model for solution of heat transfer and fluid flow in the weldment.

based on the nature of the flow in a given system. An effective thermal conductivity is determined similarly. The turbulent thermal conductivity and the turbulent viscosity are related by the turbulent Prandtl number (Pr_t), which is defined in the following relation:

$$Pr_t = \frac{C_p \mu_t}{k_t} = 0.9 \qquad [19]$$

where C_p is the specific heat of the liquid iron, μ_t is the turbulent viscosity, and k_t is the turbulent thermal conductivity. The turbulent Prandtl number is held constant at a value of 0.9 for these calculations.

The effect of turbulent flow on the transport of nitrogen in the weld-pool has also been considered. In order to enhance the transport of nitrogen with the presence of turbulence, the diffusion coefficient has been enhanced. By enhancing the diffusion coefficient, the ratio between the effective and theoretical diffusivity for nitrogen in liquid iron (D_{eff}/D_N) is defined. For the following calculations, the nitrogen diffusion coefficient in liquid iron is enhanced by a constant factor of 20.

D. *Boundary Conditions*

The boundary conditions for the steady-state solution of the equations of conservation of mass, momentum, and energy are shown in Figure 2. In the solid portion of the weldment, all velocities (u, v, and w) are set equal to zero, and the initial temperature is set at 298 K. The top surface of the solution geometry is considered to be flat, and the flow of liquid out of the face is not permitted. Specifically, the gradients of the u and v velocity components are tied to the spatial gradient of the surface tension, as shown in Figure 2, and the z-component of the velocity, w, is zero. Along the plane of symmetry through the weld-pool center, similar conditions, which are specifically shown in Figure 2, are prevalent.

The distribution of the heat flux from the arc is assumed to be Gaussian in nature. The energy flux from the arc to the weld metal is prescribed on the top surface by the relationship shown in Figure 2. Knowledge of the arc efficiency is an important consideration in the calculation of heat transfer and fluid flow in the weld-pool. Previous studies have investigated the efficiency of various welding processes using calorimetry.[55] In general, the maximum efficiency of the GTA welding process has been measured to be approximately 80 pct, which is assumed to be the arc efficiency in this case. Heat transfer in the liquid-metal portion of the weldment on the top surface is defined by the relationship shown in Figure 2. On the sample surfaces, the temperature is initially set at 298 K and is maintained at this level at the surfaces far from the heat source. On the plane of symmetry, the temperature gradient is set to zero.

In addition to the initial and boundary conditions for the solution of the heat-transfer and fluid-flow calculations, similar conditions must be imposed on the solution of the nitrogen concentration. An initial nitrogen concentration of 20 ppm, which is the initial nitrogen concentration in the base metal used in the experiments, is assumed throughout the weldment. Along the plane of symmetry, the nitrogen-concentration gradient (dc/dy) is zero. Nitrogen concentrations at locations away from the sample surface and the weld-pool are prescribed to be equal to the initial nitrogen concentration of the base metal ([N] = 20 ppm).

III. EXPERIMENTAL METHODS

A series of autogeneous, bead-on-plate GTA welds have been made on nearly pure iron samples, with only trace levels of alloying elements, as shown in Table IV. Samples of this purity were used in order to avoid the effects of additional alloying elements on the nitrogen solubility. A summary of the welding conditions studied here is also included in Table IV. The effects of changes in the travel speed and shielding-gas composition on the resulting nitrogen concentration have been studied.

A schematic diagram of the welding chamber is shown in Figure 3. Within the chamber, the welding head and electrode are maintained stationary, and the sample is fastened to a computer-controlled stage that controls travel

Table IV. Experimental Welding Parameters Considered in This Study

Welding Parameters	Condition 1	Condition 2
Arc current (A)	150	150
Arc voltage (V)	25	25
Arc length (m)	0.0032	0.0032
Total pressure (MPa)	0.1	0.1
Travel speed (m/s)	0.0085	0.0042
Electrode diameter (m)	0.0024	0.0024
Ar-N_2 shielding gas mixture (vol pct)	0 to 20 pct	0 to 20 pct
Chemical composition of base plate (wt pct)	Fe	
	0.031Al	
	0.002C	
	0.0022Cr	
	0.20Mn	
	0.003Mo	
	0.006Ni	
	0.002N	
	0.002O	
	0.006P	
	0.001S	
	0.009Si	

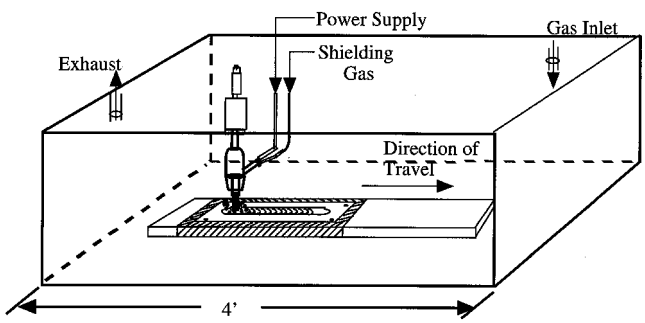

Fig. 3—Schematic diagram of experimental chamber used for controlled GTA welding experiments.

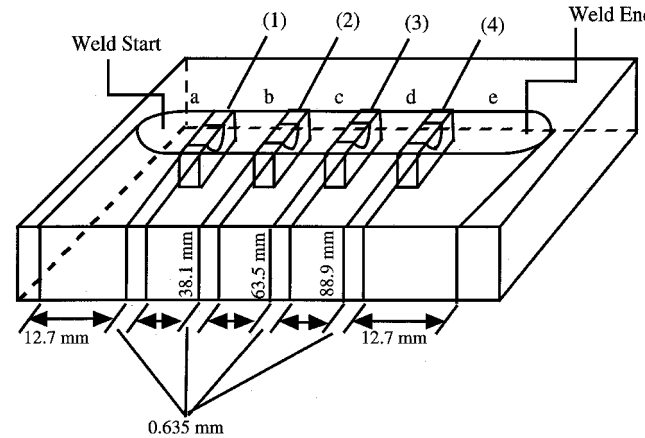

Fig. 4—Schematic representation of location of samples along weld line removed for nitrogen concentration analysis.

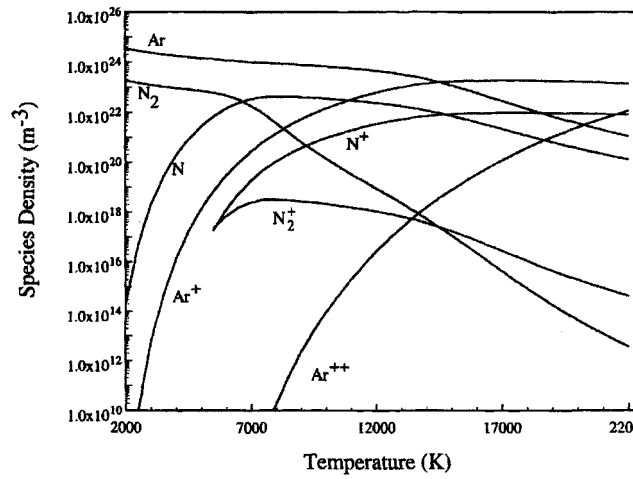

Fig. 5—Plots of computed species densities for an Ar-5 pct N_2 gas mixture as a function of temperature.

speed. The distance between the electrode tip and the workpiece, defined as the arc length, is maintained constant throughout the welding runs, and a 2 pct thoriated tungsten nonconsumable electrode, with a diameter of 0.00024 m, has been used. In order to avoid contamination of the shielding gas and weld-pool by the surrounding atmosphere, the chamber has been back-filled with argon prior to welding to purge the system of unwanted environmental impurities. Throughout the duration of each welding run, a total pressure of 0.1 MPa was maintained within the experimental chamber. Shielding of the weld-pool is provided by the use of controlled argon-nitrogen gas mixtures as the weld shielding gas. In all cases, ultra-high-purity argon and nitrogen gases are used. These gases contain extremely low quantities of impurities, thus increasing the controls on the experiments and decreasing any factors that may unduly affect the nitrogen concentration results.

After the completion of each weld line, several samples were removed from the weld line for analysis. Figure 4 shows a schematic drawing of the locations of the samples. All of these samples are 0.00064 m in thickness and are located at 0.013, 0.038, 0.064, and 0.089 m from the starting point of the weld line. The weld-metal nitrogen concentration in each of these samples was then measured using vacuum fusion analysis. Samples at the various locations on each weld line were analyzed, in order to detect any variation in the nitrogen concentration along the length of the weld line.

IV. RESULTS AND DISCUSSION

A. *Nitrogen in the Plasma Phase*

Using the calculation methodology discussed previously, the number densities for the species present in the argon-nitrogen gas mixtures of interest have been calculated. Figure 5 shows a plot of the calculated species-density distribution as a function of temperature for an Ar-5 pct N_2 gas mixture at atmospheric pressure. Similar plots can be made for the other Ar-N_2 mixtures of interest here. These plots provide insight into the effects of changes in electron temperatures in the plasma on the resulting species distributions. For example, in Figure 5, argon species dominate across the range of temperatures considered, given the much higher fraction of argon in the gas mixture. Among the nitrogen species, diatomic nitrogen dominates at temperatures below 6000 K, where the extent of dissociation and ionization is

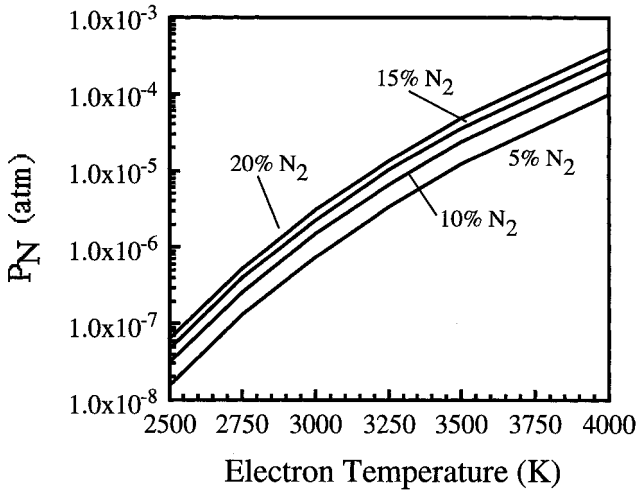

Fig. 6—Graph showing dramatic changes in monatomic nitrogen partial pressures with rather small changes in the electron temperature. The electron temperature range shown in this figure matches those temperatures found in the anode boundary layer.

low. In this temperature range, ionized species play no role and are not considered. Above approximately 7000 K, monatomic nitrogen is the dominant species, and N^+ dominates as the temperature is increased above 17,000 K. Although Figure 5 shows computed species densities only for the Ar-5 pct N_2 gas mixture, the general trends shown in this figure are representative of all gas compositions studied here.

The behavior of monatomic nitrogen, which is the dominant species in the nitrogen dissolution reaction,[4,6–8,56] is of greatest interest here. The partial pressure of monatomic nitrogen above the weld-pool is based on the electron-temperature distribution and the accompanying monatomic nitrogen species density in the plasma phase. Temperatures in the arc column have been found to range from approximately 3000 to 20,000 K, with higher temperatures near the electrode and lower temperatures at the weld-pool surface.[57–63] As the weld-pool surface is approached, though, the characteristics of the plasma phase in the arc column significantly change. This region is typified by temperatures that are significantly less than those found in the arc column and approach those on the weld-pool surface.[64]

Calculations of the monatomic nitrogen partial pressures are shown in Figure 6 as a function of the electron temperature typical of the region adjacent to the weld-pool surface for several Ar-N_2 gas mixtures. Even though only a narrow temperature range is shown here, monatomic nitrogen partial pressures vary by up to five orders of magnitude. Therefore, even small variations in the temperature directly above the weld-pool can significantly affect the amount of monatomic nitrogen available to take part in the nitrogen dissolution reaction. This steep monatomic nitrogen partial-pressure dependence and a lack of knowledge of the electron temperature adjacent to the weld-pool surface further complicate the modeling of the nitrogen dissolution reaction.

B. *Temperature and Fluid-Flow Fields in the Weld Pool*

Calculations of the temperatures and velocity fields in three dimensions have been performed for each set of experimental parameters. Figure 7 shows the calculated steady-state temperature and fluid-flow fields in the weld-pool in three dimensions, for a travel speed of 0.0085 m/s. Similar calculations have been performed for a travel speed of 0.0042 m/s. In each case, the elongated pool shapes and temperature fields are typical of welds with a moving heat source. At each travel speed, the temperature gradients are greater in front of the heat source than behind it. Computed values of the peak temperature, maximum velocities, and the weld-pool depth and width are listed in Table V for each travel speed investigated here. The effect of the change in travel speed is evident. For example, the calculated peak temperatures and weld-pool widths and depths are greater at the slower travel speed. These results are consistent with those observed in previous modeling efforts.[32]

The temperature distribution on the weld-pool surface contributes to the amount of nitrogen absorbed from the plasma phase. Figure 8 shows the weld-pool surface-temperature distribution calculated for a travel speed of 0.0085 m/s. This figure shows a rather symmetrical temperature distribution, with the peak temperatures present under the heat source and decreasing temperatures observed as the weld-pool periphery is approached. Similar behavior is also observed with a travel speed of 0.0042 m/s, except that higher temperatures are observed with the slower travel

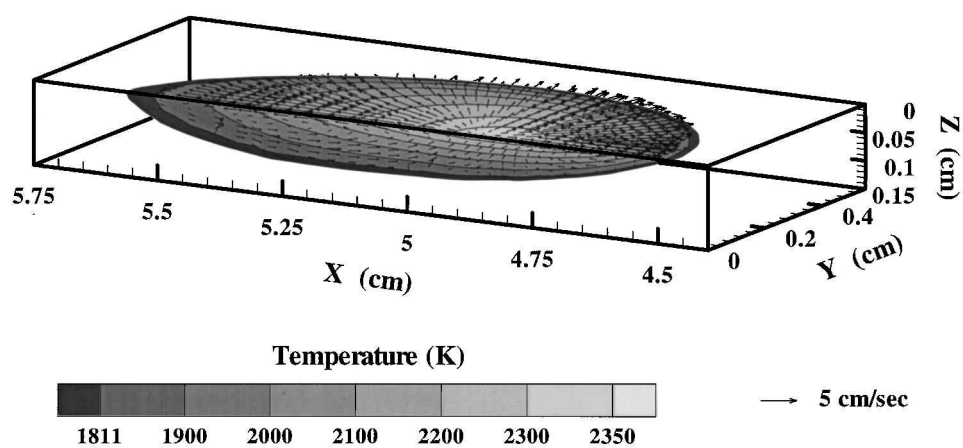

Fig. 7—Three-dimensional diagram showing modeling results for both temperature and fluid flow fields in the weld-pool for a travel speed of 0.0085 m/s.

Table V. Summary of Output Data from These Calculations

	Condition 1	Condition 2
Peak temperature (K)	2377	2551
Maximum velocities (m/sec)		
u_{max}	0.064	0.11
v_{max}	0.083	0.12
w_{max}	0.011	0.017
Weld-pool depth (m)	0.00077	0.001
Weld-pool width (m)	0.0073	0.010
Number of grids	62400	62400

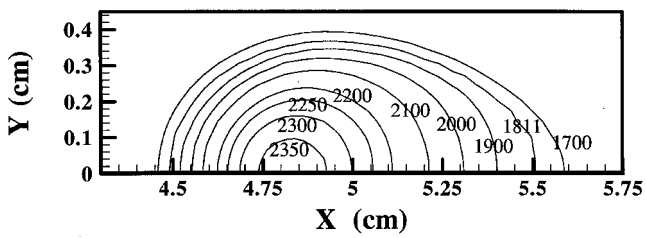

Fig. 8—Computed temperature profiles on the weld-pool surface for a travel speed of 0.00847 m/s. All temperatures are in degrees Kelvin.

speed. Changes in the temperature distribution on the weld-pool surface affect the resulting nitrogen absorption and the spatial distribution of nitrogen concentrations.

The calculated weld-pool dimensions are compared with the corresponding experimental values at a travel speed of 0.0085 m/s in Figure 9. The calculated dimensions generally correspond with the experimental weld-pool shape, even though the modeled weld-pool is somewhat wider. Velocity fields in the weld-pool cross section are also shown in Figure 9. In each case, a strong outward flow of liquid from the weld-pool center to the weld-pool periphery is observed at each travel speed. This behavior is indicative of a metal with low concentrations of surface-active elements and is consistent with previous modeling[32] and experimental[65] work. The nitrogen-concentration distributions resulting from these changes in temperature and the monatomic nitrogen partial pressure are discussed in Section C.

C. *Nitrogen Surface Concentrations*

Nitrogen concentrations on the weld-pool surface are based on both the monatomic nitrogen partial pressures above the weld-pool and the weld-pool surface temperatures. The monatomic nitrogen partial pressures, in turn, are based on the electron temperatures present in the plasma phase and the nitrogen addition to the shielding gas. In this study, electron temperatures are assumed to be between 2500 and 4000 K. This choice of temperature is based, in part, on previous experimental measurements[58–63] of the temperature distribution in the welding arc, which show electron temperatures in the range of 5000 K close to the weld-pool surface. Furthermore, our previous calculations show that, with an Ar-1 pct N_2 gas mixture, the weld-pool surface becomes saturated with nitrogen[19] at electron temperatures of 5000 K. For gas mixtures containing higher percentages of nitrogen, the saturation occurs at lower electron temperatures. Therefore, the effects of electron temperatures below this level are investigated here.

A distribution of electron temperatures is also assumed to exist above the weld-metal surface. For example, a maximum electron temperature is located directly under the heat source, and a minimum value occurs at the solid-liquid interface. This variation is based on the change in electron temperatures in the plasma phase as the distance from the energy source is increased. The magnitude of this temperature variation is expected to be rather small, given the small size of the weld-pools examined here. Therefore, the effects of electron temperature variations of 250 and 500 K have been examined here. An example of the electron-temperature distributions analyzed here is shown in Figure 10(a), for an electron-temperature distribution between 3250 and 3000 K at a travel speed of 0.0085 m/s. Similar electron-temperature distributions are observed with each electron-temperature range examined here. When the travel speed is decreased, the electron-temperature range is distributed over the larger size of the weld-pool.

These electron-temperature distributions are then used as a basis for determining the monatomic nitrogen partial pressures above the weld-pool. Table VI summarizes the minimum and maximum electron temperatures and the corresponding monatomic nitrogen partial pressures. It is observed that even small changes in the electron temperature can produce changes in the monatomic nitrogen partial pressure of between a factor of 3 and 10. The monatomic nitrogen partial-pressure distribution, based on the electron-temperature distribution in Figure 10(a), is shown in Figure 10(b) with an Ar-10 pct N_2 shielding gas mixture. The monatomic nitrogen partial-pressure distribution is closely related to the electron-temperature distribution, with higher monatomic nitrogen partial pressures present in areas with higher electron temperatures and decreasing monatomic nitrogen partial pressures present at the periphery of the weld-pool.

Nitrogen concentrations on the weld-pool surface can then

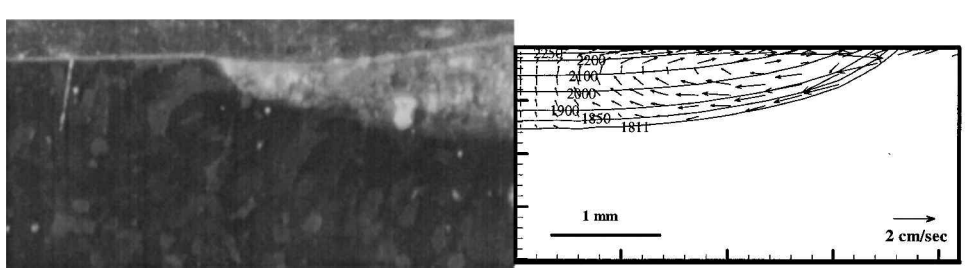

Fig. 9—Comparison between the experimental and calculated weld-pool cross sections at a travel speed of 0.00847 m/s.

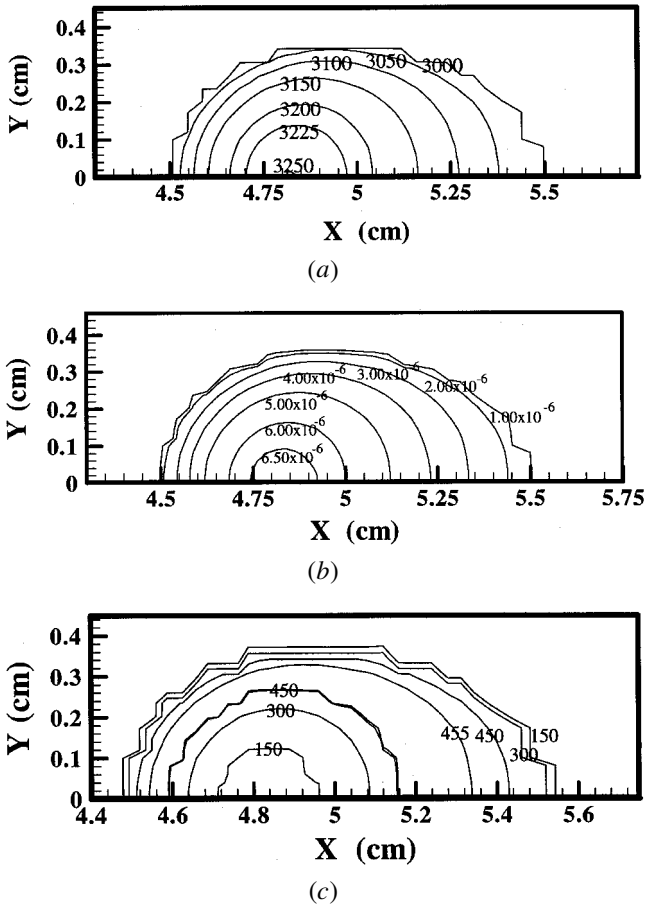

Fig. 10—(*a*) Electron temperature (K), (*b*) monatomic nitrogen partial pressure (atm), and (*c*) nitrogen concentration (ppm) distributions for a travel speed of 0.0085 m/s and a 10 pct N_2 addition to the shielding gas. A maximum temperature of 3250 K and a minimum temperature of 3000 K are considered.

be calculated by combining the surface-temperature distribution with the monatomic nitrogen partial-pressure distribution above the weld-pool. Figure 10(c) shows the calculated nitrogen concentrations on the weld-pool surface for the conditions described in Figures 10(a) and (b). A similar pattern emerges for each electron-temperature distribution. At the weld-pool center, the nitrogen concentrations are their lowest, even though the monatomic nitrogen partial pressures are at a maximum. As the weld-pool periphery is approached, the nitrogen concentrations reach a maximum value, equal to the level at which nitrogen desorption occurs. This nitrogen concentration is defined by Sieverts law at the surface temperature and at a nitrogen partial pressure of 0.1 MPa.[4,18,19] For example, the nitrogen concentration in liquid iron at a temperature of 1873 K and a total pressure of 0.1 MPa is approximately 450 ppm. The overall behavior observed here is indicative of the solubility of nitrogen in iron due to monatomic species, in which the nitrogen solubility decreases with an increase in the temperature of the liquid iron.[23]

Changes in either the electron-temperature distribution or the nitrogen addition to the shielding gas also affect the nitrogen surface concentrations. In each case, changes in either of these parameters result in changes in the monatomic nitrogen partial pressures above the weld-pool. Lower electron temperatures translate into lower nitrogen concentrations on the weld-pool surface, while higher electron temperatures result in higher nitrogen concentrations. The nitrogen-concentration distribution noticeably changes with the addition of more nitrogen to the shielding gas. Nitrogen concentrations at the level of nitrogen desorption are present over a larger proportion of the weld-pool surface. Higher nitrogen concentrations are also present in the region directly under the heat source, never reaching the levels observed on the weld-pool periphery.

D. *Nitrogen Concentrations in the Weld Pool*

Nitrogen absorbed on the weld-pool surface is transported to the weld-pool interior by convection and diffusion. Therefore, the nitrogen concentrations on the weld-pool surface have a significant impact on the resulting nitrogen concentrations in the weld-pool interior. Three-dimensional, transient calculations of the nitrogen concentrations in the weld-pool have been performed here. A typical nitrogen-concentration distribution in the weld-pool is shown in Figure 11 for a travel speed of 0.0085 m/s, a 10 pct N_2 addition to the shielding gas, and electron temperatures between 3250 and 3000 K. In this figure, the transient

Table VI. Summary of Electron Temperature and Monatomic Nitrogen Partial Pressure (P_N) Distributions

Electron Temperatures		5 Pct N_2		10 Pct N_2		15 Pct N_2		20 Pct N_2	
Maximum	Minimum	P_N Max (MPa)	P_N Min (MPa)	P_N Max (MPa)	P_N Min (MPa)	P_N Max (MPa)	P_N Min (MPa)	P_N Max (MPa)	P_N Min (MPa)
250K difference									
3500 K	3250 K	1.21×10^{-4}	3.36×10^{-5}	2.42×10^{-4}	6.73×10^{-5}	3.63×10^{-4}	1.01×10^{-4}	4.83×10^{-4}	1.35×10^{-4}
3250 K	3000 K	3.36×10^{-5}	7.58×10^{-6}	6.73×10^{-5}	1.52×10^{-5}	1.01×10^{-4}	2.27×10^{-5}	1.35×10^{-4}	3.03×10^{-5}
3000 K	2750 K	7.58×10^{-6}	1.31×10^{-6}	1.52×10^{-5}	2.61×10^{-6}	2.27×10^{-5}	3.92×10^{-6}	3.03×10^{-5}	5.22×10^{-6}
2750 K	2500 K	1.31×10^{-6}	1.59×10^{-7}	2.61×10^{-6}	3.17×10^{-7}	3.92×10^{-6}	4.76×10^{-7}	5.22×10^{-6}	6.34×10^{-7}
500K difference									
4000 K	3500 K	9.69×10^{-4}	1.21×10^{-4}	1.94×10^{-3}	2.42×10^{-4}	2.91×10^{-3}	3.63×10^{-4}	3.88×10^{-3}	4.83×10^{-4}
3500 K	3000 K	1.21×10^{-4}	7.58×10^{-6}	2.42×10^{-4}	1.52×10^{-5}	3.63×10^{-4}	2.27×10^{-5}	4.83×10^{-4}	3.03×10^{-5}
3250 K	2750 K	3.36×10^{-5}	1.31×10^{-6}	6.73×10^{-5}	2.61×10^{-6}	1.01×10^{-4}	3.92×10^{-6}	1.35×10^{-4}	5.22×10^{-6}
3000 K	2500 K	7.58×10^{-6}	1.59×10^{-7}	1.52×10^{-5}	3.17×10^{-7}	2.27×10^{-5}	4.76×10^{-7}	3.03×10^{-5}	6.34×10^{-7}

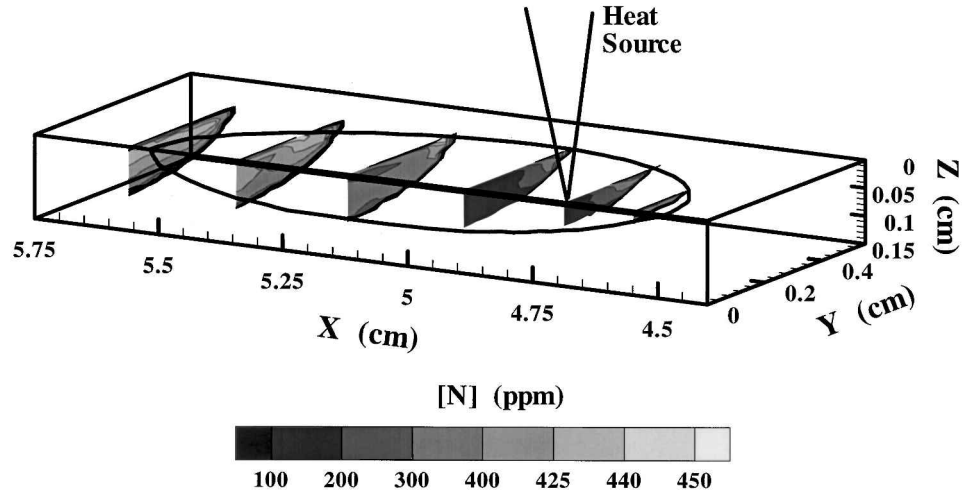

Fig. 11—Three-dimensional plot of nitrogen concentrations in the weld-pool at several times for a travel speed of 0.00847 m/s. Electron temperatures between 3250 and 3000 K for a 10 pct N_2 addition to the shielding gas are assumed.

nitrogen concentrations are superimposed on the steady-state weld-pool shape, giving an indication of how the nitrogen concentration varies up to solidification.

Nitrogen concentrations evolve along the length of the weld-pool up to the point of solidification. In the early stages of this evolution, lower nitrogen concentrations are observed in the center of the weld-pool. This behavior is a result of the lower solubility of nitrogen in liquid iron due to monatomic nitrogen at the higher temperatures present in these locations. It is also apparent that the transport of nitrogen is the result of the fluid-flow patterns in the weld metal. A radially outward flow dominates in the weld-pool, and the nitrogen concentrations present in the weld-pool are affected by this behavior. As the weld-pool evolves, the transport of nitrogen from the outer edges to the interior of the weld-pool cross section is evident.

By the time the weld-pool solidifies, the nitrogen concentration distribution is rather homogeneous. Once the weld-pool solidifies, the nitrogen is trapped in place, and this final distribution determines the residual nitrogen concentration in the weld-pool. Figure 12(a) shows a nitrogen-concentration distribution across the solidified weld-pool cross section for a 10 pct N_2 addition to the shielding gas, electron temperatures in the plasma phase between 3250 and 3000 K, and a travel speed of 0.0085 m/s. A spatial variation in the nitrogen concentration exists in the weld-pool. The highest nitrogen concentrations are located in the weld-pool center and decrease as the former liquid-solid interface is approached. In general, though, the nitrogen concentrations are rather homogenous throughout the bulk of the weld-pool, but they rapidly change at the weld-pool peripheries.

The effect of changes in the travel speed, the nitrogen addition to the shielding gas, and the electron temperatures in the plasma phase above the weld-pool on the resulting nitrogen-concentration distribution in the weld-pool have been examined here. Changes in the travel speed with all other conditions maintained constant have little effect on the resulting nitrogen-concentration distribution in the weld-pool. On the other hand, changes in the electron-temperature distribution above the weld-pool noticeably affect the calculated nitrogen-concentration distributions, as shown in Figures 12(b) and (c). Significantly higher nitrogen

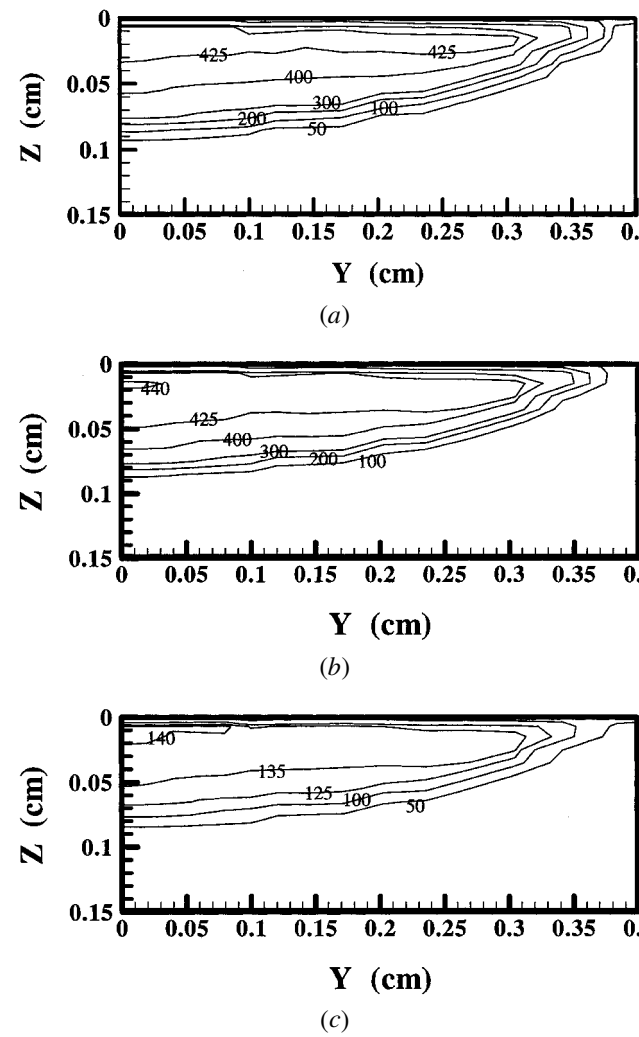

Fig. 12—Nitrogen-concentration (ppm) distributions in the weld-pool for electron temperature distribution across the weld-pool ranging between (*a*) 3250 and 3000 K, (*b*) 3500 and 3250 K, and (*c*) 2750 and 2500 K with a 10 pct N_2 addition to the shielding gas and a travel speed of 0.0085 m/s.

concentrations are observed at the higher electron temperatures. An analysis of the resulting nitrogen-concentration distributions over this electron-temperature range shows that electron temperatures above 3000 K produce similar nitrogen concentrations in the weld-pool. At these electron temperatures, there is little variation in the nitrogen surface-concentration distributions, thus leading to similar nitrogen concentrations in the weld-pool interior. Therefore, only electron temperatures between 3000 and 3250 K are considered in the remaining analysis.

The effects of different nitrogen additions to the shielding gas on the resulting nitrogen-concentration distribution in the weld-pool have also been investigated. Nitrogen concentrations in the weld-pool interior increase with an increase in the nitrogen addition to the shielding gas, but there is little change in the general shape of the nitrogen-concentration distribution. As the nitrogen addition to the shielding gas is further increased, especially in the range between 15 and 20 pct N_2 additions, nitrogen concentrations in the weld-pool approach the level required for nitrogen desorption. Changes in the nitrogen addition to the shielding gas have less of an effect on the resulting nitrogen-concentration distribution than those observed with changes in the electron temperatures. In each case, the monatomic nitrogen partial pressure is increased, but its level of increase is much less with increases in the nitrogen addition than with the changes in the electron temperatures considered here.

The residual nitrogen concentrations in the weld-pool are computed by integrating the nitrogen concentrations across the solidified weld-pool cross section. These values can then be compared with the experimental results obtained here. At each travel speed, the average nitrogen concentration generally increases with an increase in the nitrogen partial pressure. Observed nitrogen concentrations fall in a range of 2.7 to 4.7 times greater than Sieverts-law calculations at temperatures of 2000 and 2500 K and at the same nitrogen partial pressures. Therefore, temperatures on the weld-pool surface are shown to not be responsible for these nitrogen concentrations.

Nitrogen concentrations have been calculated over a range of electron temperatures and compared with these experimental results. For each set of electron temperatures and travel speeds, the calculated nitrogen concentrations increase with the nitrogen addition to the shielding gas. When higher electron temperatures are assumed to exist above the weld-pool, the magnitude of this increase becomes less and the nitrogen concentrations across the range of nitrogen additions become similar. Electron temperatures at these levels produce nitrogen concentrations on the weld-pool surface at or near the level at which nitrogen desorption is considered, allowing no more nitrogen to enter the weld-pool. On the other hand, when the calculated nitrogen concentrations are compared with the experimental results, they fall below the experimental values for each condition considered. Therefore, there are other conditions to be taken into account in the calculations.

E. *Nitrogen Desorption Effects*

Since these calculated nitrogen concentrations are less than the experimental results, other mechanisms are contributing to the nitrogen dissolution reaction. One such mechanism which contributes to the nitrogen concentration in the weld-pool is the desorption of nitrogen from the solidifying weld metal. Previous researchers[18,20,50] have addressed the role of this reaction in determining the final nitrogen concentration in the weld-pool. In this model, a limit is placed on the nitrogen concentrations in the weld-pool to define the level of nitrogen at which desorption occurs. The choice of this level is rather arbitrary, and in the previous calculations, it was set equal to the Sieverts-law calculations for nitrogen in liquid iron, with a nitrogen partial pressure of 0.1 MPa. Since this value is insufficient to explain the experimental results, the effects of changing this level of nitrogen-concentration value are examined here.

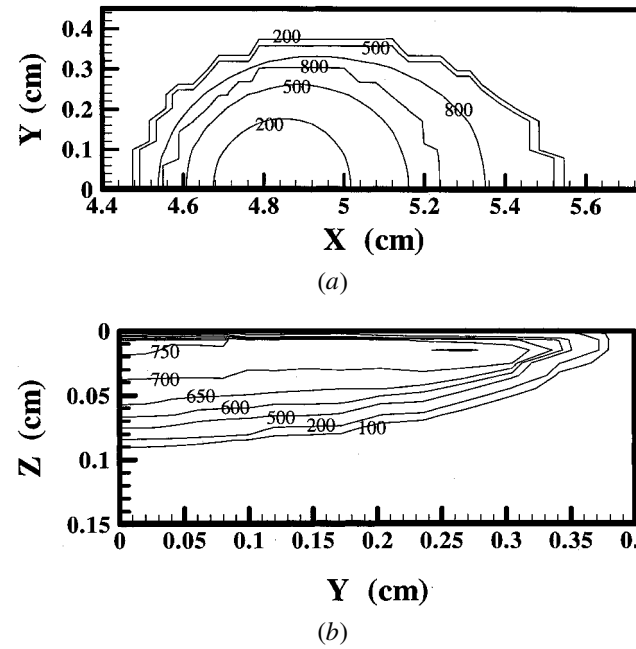

Fig. 13—Calculated Nitrogen-concentration (ppm) distributions (*a*) on the weld-pool surface and (*b*) in the weld-pool interior at a travel speed of 0.0085 m/s and a 10 pct N_2 addition to the shielding gas for an enhancement in the level of nitrogen supersaturation of 1.75.

The effect of the gas concentration in the liquid metal on the resulting desorption of gas has been noted elsewhere.[66,67] For example, during the decarburization of iron melts, ([C] + [O] → CO (g)), carbon concentrations can reach levels up to 15 times higher than those predicted by equilibrium calculations. The removal of carbon from the melt through the evolution of CO (g) from liquid iron has been found to be dependent upon the availability of nucleation sites for bubble formation within the melt. As the number of heterogeneous nucleation sites increases, the level of carbon supersaturation in the melt decreases.

In this case, nitrogen desorption ($2[N] \rightarrow N_2$ (g)) is tied to a supersaturation of nitrogen in the liquid iron. This level of nitrogen supersaturation is not well defined, and the effect of several nitrogen supersaturation levels ranging between 25 and 100 pct higher than the nitrogen solubility calculated by Sieverts-law calculations, for a nitrogen partial pressure of 1 atm, have been analyzed. In Figures 13(a) and (b), the effects of nitrogen supersaturation enhancements of 75 pct on the resulting nitrogen-concentration distributions on the weld-pool surface and in the weld-pool interior, respectively, are shown. Electron temperatures between 3250 and 3000 K are analyzed here, because the calculated nitrogen surface

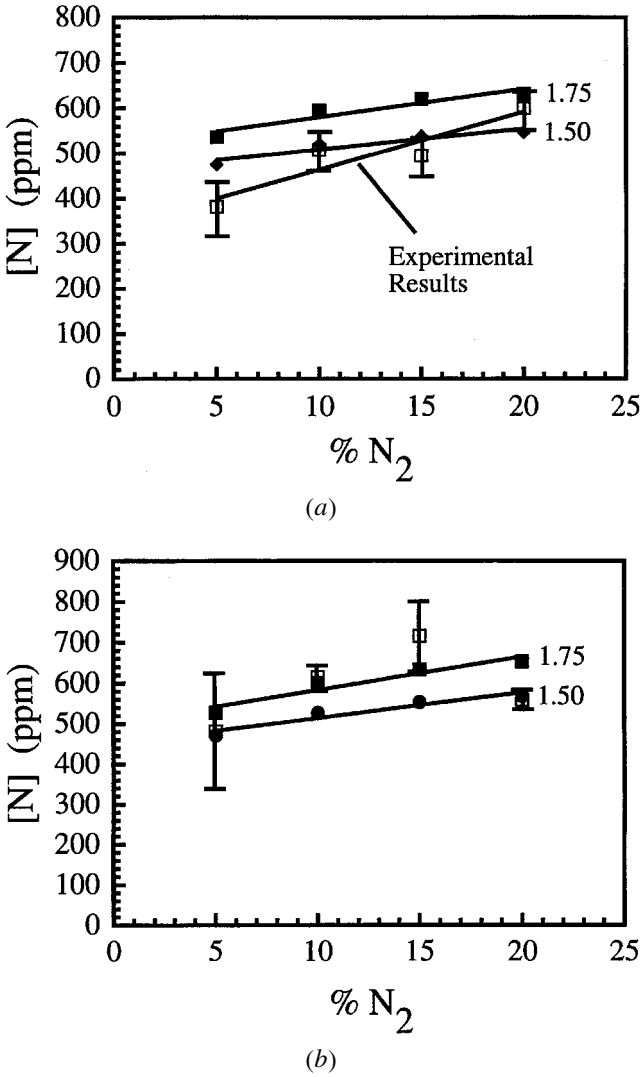

Fig. 14—Comparison between experimental and calculated nitrogen concentrations over a range of nitrogen additions to the shielding gas for several levels of nitrogen supersaturation for a travel speed of (*a*) 0.0085 m/s and (*b*) 0.0042 m/s for an electron temperature range between 3250 and 3000 K.

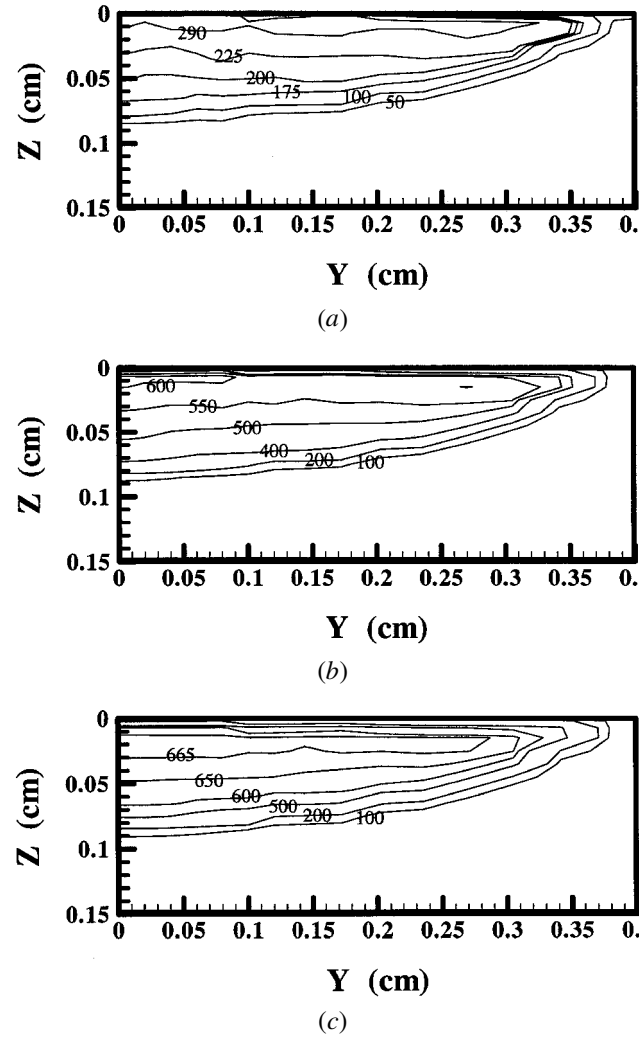

Fig. 15—Summary of final nitrogen-concentration (ppm) distributions for several diffusive mass transport enhancement factors for a travel speed of 0.0085 m/s and a 10 pct N_2 addition to the shielding gas for electron temperatures ranging from 3250 to 3000 K: (*a*) 1, (*b*) 10, and (*c*) 50. A nitrogen supersaturation level of 50 pct is assumed.

concentrations are near the levels of nitrogen saturation defined by Sieverts law in the previous section.

With a 75 pct enhancement in the maximum allowable nitrogen concentration on the weld-pool surface, significantly higher nitrogen concentrations are present on the weld-pool surface and in the weld-pool interior. For example, nitrogen concentrations on the weld-pool surface reach levels approaching 800 ppm [N] near the weld-pool periphery and 750 ppm [N] in the weld-pool interior for the conditions shown in Figures 13(a) and (b). Even though these levels are significantly higher than those observed in previous calculations, there is minimal difference in the general trends observed on either the weld-pool surface or in the weld-pool interior, when no supersaturation is assumed. Similar conditions are observed with each level of nitrogen supersaturation examined at each travel speed and with each nitrogen addition to the shielding gas.

A comparison between the calculated nitrogen concentrations and the experimental results is shown in Figures 14(a) and (b), as a function of the nitrogen additions to the shielding gas for each travel speed. The effects of several enhancements in the nitrogen saturation levels are also shown. Unlike previous comparisons between experimental and calculated results, the calculated results for enhancements between 50 and 75 pct fall in the same range as the experimentally observed results for each travel speed. For each level of enhancement, the calculated nitrogen concentrations increase with greater additions of nitrogen to the shielding gas. This generally linear increase in the calculated nitrogen concentration provides a similar trend to that observed experimentally. Therefore, the consideration of nitrogen desorption through an increase in the allowable nitrogen concentrations on the weld-pool surface provides a necessary component to this model and enhances the understanding of the nitrogen dissolution reaction.

F. *Effect of Turbulence*

In the previous calculations, the presence of turbulence in the weld-pool was taken into account. Little is known, though, about the quantitative role of turbulence on the

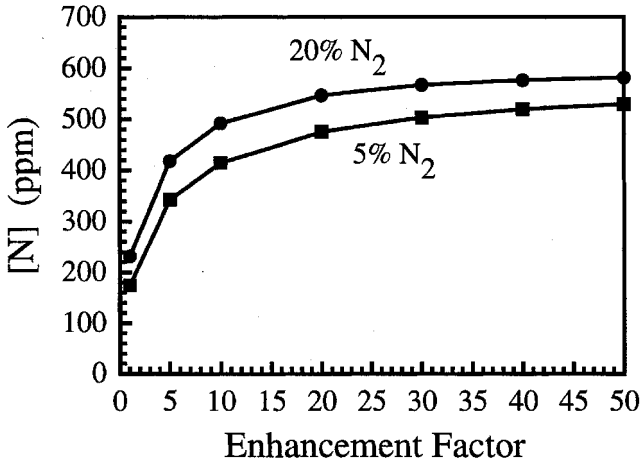

Fig. 16—Summary of calculated nitrogen concentrations for a number of enhancement factors to the diffusion coefficient for a travel speed of 0.0085 m/s and 5 and 20 pct N_2 additions to the shielding gas and an electron temperature distribution above the weld-pool ranging from 3250 to 3000 K and a 50 pct nitrogen supersaturation level.

transport of nitrogen in the weld-pool and the resulting nitrogen-concentration distribution. One way to take into account this agitated or turbulent fluid flow is to enhance the diffusion coefficient. This concept is based on previous work, which took into account the role of convection in the weld-pool and its effect on heat transfer by enhancing the thermal-conductivity value.[52] Calculations are made with several enhancements to the nitrogen diffusion coefficient at each travel speed and with nitrogen supersaturation levels between 50 and 75 pct. Figures 15(a) through (c) show the final calculated nitrogen-concentration distributions in the weld-pool for several levels of enhancement to the nitrogen diffusion coefficient and at a nitrogen supersaturation of 50 pct. Nitrogen concentrations increase throughout the weld-pool with each enhancement of the nitrogen diffusion coefficient.

The effects of enhancing the nitrogen diffusion coefficient on the residual nitrogen concentration at a constant nitrogen addition are shown in Figure 16 for 5 and 20 pct N_2 additions to the shielding gas and at a nitrogen supersaturation of 50 pct. In this figure, enhancements in the nitrogen diffusion coefficient produce a corresponding increase in the residual nitrogen concentration at a constant nitrogen addition to the shielding gas. With a significant increase in the nitrogen addition to the shielding gas, there is little increase in the residual nitrogen concentration. Changes in the travel speed and level of nitrogen supersaturation do not affect the behavior shown in Figure 16 as a function of the enhancement of the nitrogen diffusion coefficient. These results indicate that changes in the nitrogen diffusion coefficient do not affect the basic nitrogen transport mechanisms in the weld-pool, but, rather, only further enhance the mixing in the weld-pool.

Calculated and experimental nitrogen concentrations for each travel speed and with several enhancements to the nitrogen diffusion coefficient are compared in Figures 17(a) and (b) for nitrogen supersaturations of 75 pct. In each case, changes in the nitrogen diffusion coefficient affect the resulting residual nitrogen concentration. For example, the nitrogen concentrations with no enhancement to the nitrogen diffusion coefficient are significantly lower than the experimental results. When the nitrogen diffusion coefficient is

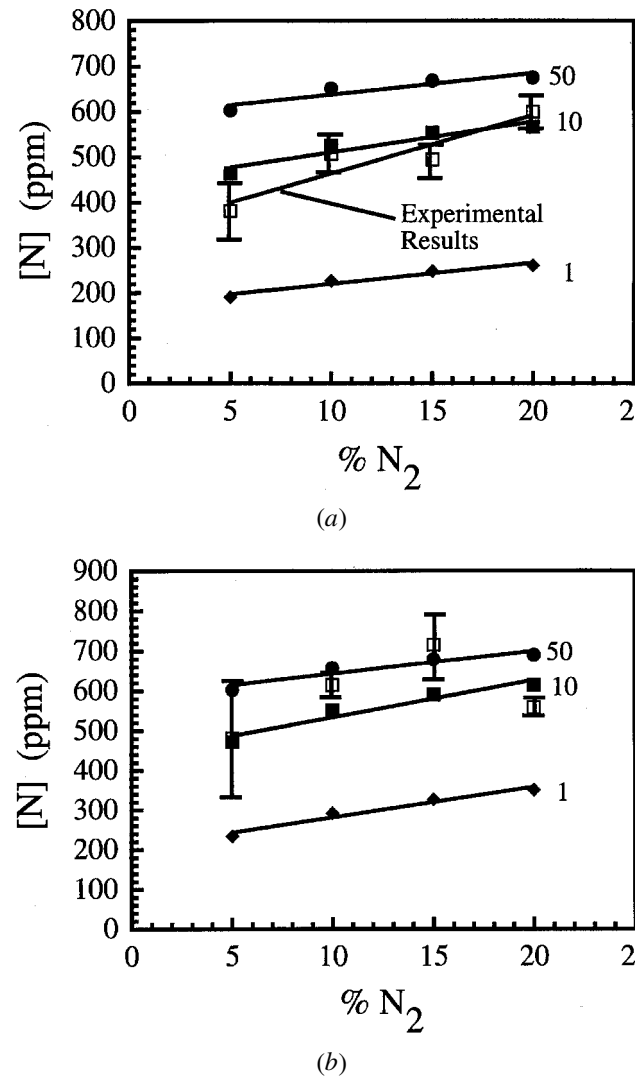

Fig. 17—Comparison between experimental nitrogen concentrations and modeled results for several mass transport enhancement factors at electron temperatures between 3250 and 3000 K for a nitrogen supersaturation level of 75 pct at a travel speed of (*a*) 0.0085 m/s and (*b*) 0.0042 m/s.

enhanced, the calculated residual nitrogen concentrations fall in the range of the experimental results. At enhancements of 10 and above, though, there is little difference in the resulting nitrogen concentrations. Taken as a whole, turbulence is an important component in the calculation of the nitrogen concentration, but the choice of the level of enhancement in the diffusion coefficient appears insignificant, as long as the value is 10 or above.

V. SUMMARY AND CONCLUSIONS

A model to calculate the nitrogen concentration in the weld metal during the GTA welding of iron is developed here. The calculation of the nitrogen concentrations in the weld-pool is based on a combination of calculations involving the plasma phase above the weld-pool, the interface between the weld-pool surface and the plasma phase, and the weldment interior. Monatomic nitrogen partial pressures are calculated as a function of the electron temperatures in the plasma phase using

the calculation methodology discussed here. Nitrogen concentrations on the weld-pool surface are calculated as a function of both the monatomic nitrogen partial pressure and the weld-pool surface temperatures. Once absorbed at the weld-pool surface, nitrogen is then transported predominantly by convection to the weldment interior. The presence of turbulence in the weld-pool, which is taken into account by increasing the nitrogen diffusion coefficient, further enhances the transport of nitrogen. Nitrogen desorption, which occurs *via* bubble formation at the liquid-metal surface, is characterized by a supersaturation of nitrogen in the weld metal and is also considered in this model.

To test the validity of this model, several autogeneous GTA welding experiments in pure iron have been performed at two travel speeds, with a number of nitrogen additions to the argon shielding gas. Nitrogen concentrations have also been measured at several locations along each weld line and compared with the modeling results. The general shape and size of the experimental and modeled weld-pools are similar. Both the modeling and experimental results produce nitrogen concentrations between 2.7 and 4.7 times higher than Sieverts-law calculations for a temperature of 2000 K and nitrogen partial pressures between 0.005 and 0.020 MPa. When the modeling and experimental results are compared, both results are equivalent in magnitude for a given set of welding parameters and follow similar trends with changes in the nitrogen addition to the shielding gas and the travel speed.

The modeling calculations also display several features that contribute to these results. Electron temperatures in the plasma phase adjacent to the weld-pool, in a range around 3000 K, are found to produce levels of monatomic nitrogen sufficient to produce nitrogen concentrations in the weld-pool equivalent to the experimental results. Levels of nitrogen supersaturation, which are between 50 and 75 pct higher than the equilibrium nitrogen concentration, are required to produce the nitrogen concentrations equivalent to the experimental results. The incorporation of turbulence in the calculations is important to the final results for each travel speed. On the other hand, enhancements to the diffusion coefficient above a factor of 20 have little effect.

ACKNOWLEDGMENTS

This work was supported by the United States Department of Energy, Office of Basic Energy Sciences, Division of Materials Science, under Grant No. DEFG02-84ER45158. Dr. T.A. Palmer also acknowledges the financial support provided by the American Welding Society Foundation and the Navy Joining Center in the form of an AWS Graduate Research Fellowship.

REFERENCES

1. S. Kou: *Welding Metallurgy*, John Wiley and Sons, New York, NY, 1987, pp. 61-63.
2. C.J. Allum: *Bull. Welding Res. Council*, 1991-92, vol. 369, pp. 68-84.
3. P.D. Blake: *Weld. Res. Int.*, 1979, vol. 9 (1), pp. 23-56.
4. T.A. Palmer, K. Mundra, and T. DebRoy: in *Mathematical Modelling of Weld Phenomena 3*, H. Cerjak, ed., The Institute of Materials, London, 1997, pp. 3-40.
5. T. Kuwana: *Advanced Joining Technologies. Proc. Int. Institute of Welding Congr. on Joining Research*, T.H. North, ed., Chapman and Hall, New York, 1990, pp. 117-28.
6. T. Kuwana, H. Kokawa, and M. Saotome: in *Mathematical Modelling of Weld Phenomena 3*, H. Cerjak, ed., The Institute of Materials, London, 1997, pp. 64-81.
7. T. Kuwana and H. Kokawa: *Trans. Jpn. Weld. Soc.*, 1986, vol. 17 (1), pp. 20-26.
8. T. Kuwana, H. Kokawa, and K. Naitoh: *Trans. Jpn. Weld. Soc.*, 1990, vol. 21 (2), pp. 85-91.
9. T.A. Palmer and T. DebRoy: *Weld. J.*, 1996, vol. 75 (6), pp. 197-s-207-s.
10. F. Elliott and M. Gleiser: *Thermochemistry for Steelmaking I*, Addison-Wesley Publishing Co., Reading, MA, 1963, p. 75.
11. *The Making, Shaping and Treating of Steel*, 9th ed, H.E. McGannon, ed., Association of Iron and Steel Engineers, Pittsburgh, PA, 1971, pp. 330-31.
12. G. den Ouden and O. Griebling: in *Recent Trends in Welding Science and Technology*, S.A. David and J.M. Vitek, eds., ASM INTERNATIONAL, Materials Park, OH, 1990, pp. 431-35.
13. F.S. Death and D.A. Haid: U.S. Patent No. 3,257,197, 1966.
14. V.I. Lakomskii and G.F. Torkhov: *Sov. Phys. Dokl.*, 1969, vol. 13 (11), pp. 1159-61.
15. J.D. Katz and T.B. King: *Metall. Trans. B*, 1989, vol. 20B, pp. 175-85.
16. T. Kuwana and H. Kokawa: *Trans. Jpn. Weld. Soc.*, 1988, vol. 19 (2), pp. 12-19.
17. P.D. Blake and M.F. Jordan: *J. Iron Steel Inst.*, 1971, vol. 209 (3), pp. 197-200.
18. K. Mundra and T. DebRoy: *Metall. Mater. Trans.*, 1995, vol. 26B, pp. 149-58.
19. T.A. Palmer and T. DebRoy: *Sci. Technol. Welding Joining*, 1998, vol. 3 (4), pp. 190-203.
20. M. Uda and S. Ohno: *Trans. Nat. Res. Inst. Met.*, 1978, vol. 20 (6), pp. 358-65.
21. K. Takeda and Y. Nakamura: *Trans. Iron Steel Inst. Jpn.*, 1978, vol. 18, pp. 641-47.
22. S. Ohno and M. Uda: *Trans. Nat. Res. Inst. Met.*, 1981, vol. 23 (4), pp. 243-48.
23. M. Uda and T. Wada: *Trans. Nat. Res. Inst. Met.*, 1968, vol. 10 (2), pp. 21-33.
24. S.A. Gedeon and T.W. Eagar: *Weld. J.*, 1990, vol. 69, pp. 264s-271s.
25. G.J. Dunn and T.W. Eagar: *Metall. Trans. A*, 1986, vol. 17A, pp. 1865-71.
26. K.S. Drellishak, D.P. Aeschliman, and A.B. Cambel: *Phys. Fluids*, 1965, vol. 8 (9), pp. 1590-1600.
27. K.S. Drellishak, C.F. Knopp, and A.B. Cambel: *Phys. Fluids*, 1963, vol. 6 (9), pp. 1280-88.
28. J.D. Fast: *Philips Res. Rep.*, 1947, vol. 2, pp. 382-98.
29. J.D. Fast and M.B. Verrijp: *J. Iron Steel. Inst.*, 1955, vol. 180, pp. 337-43.
30. R.B. McLellan and K. Alex: *Scripta Metall.*, 1970, vol. 4, pp. 967-70.
31. R.D. Pehlke and J.F. Elliott: *Trans. AIME*, 1960, vol. 218, pp. 1088-1101.
32. K. Mundra, T. DebRoy, and K.M. Kelkar: *Num. Heat Transfer A*, 1996, vol. 29, pp. 115-29.
33. K. Mundra, J.M. Blackburn, and T. DebRoy: *Sci. Technol. Welding Joining*, 1997, vol. 2 (4), pp. 174-84.
34. S. Kou and Y.H. Wang: *Metall. Trans. A*, 1986, vol. 17A, pp. 2265-70.
35. C. Prakash, M. Sammonds, and A.K. Singhal: *Int. J. Heat Mass Transfer*, 1987, vol. 30 (12), pp. 2690-94.
36. E.T. Turkdogan: in *BOF Steelmaking*, R.D. Pehlke *et al.*, ISS-AIME, New York, NY, 1975, pp. 1-190.
37. *Smithells Metals Reference Book*, 6th ed., E.A. Brandes and G.B. Brook, ed., Butterworth and Co., London, 1983.
38. M.W. Chase, Jr., C.A. Davies, J.R. Downey, Jr., D.J. Frurip, R.A. McDonald, and A.N. Syverud: *JANAF Thermochemical Tables*, 3rd ed., American Chemical Society and American Institute for Physics, Washington, DC, 1985.
39. Z. Yang and T. DebRoy: *Metall. Mater. Trans. B*, 1999, vol. 30B, pp. 483-93.
40. Z. Yang: University Park, PA, Ph. D. Thesis, The Pennsylvania State University, 2000.
41. S.A. David and T. DebRoy: *Science*, 1992, vol. 257, pp. 497-502.
42. T. DebRoy and S.A. David: *Rev. Mod. Phys.*, 1995, vol. 67 (1), pp. 85-112.
43. A. Paul and T. DebRoy: *Metall. Trans. B*, 1988, vol. 19B, pp. 851-58.
44. M.L. Wasz and R.B. McLellan: *Scripta Metall. Mater.*, 1993, vol. 28, pp. 1461-63.

45. P. Grieveson and E.T. Turkdogan: *Trans. TMS-AIME*, 1964, vol. 230, pp. 1604-09.
46. K. Schwerdtfeger: *Trans. TMS-AIME*, 1967, vol. 239, pp. 134-38.
47. *The Making, Shaping, and Treating of Steel*, 10th ed., H.E. McGannon, ed., Association of Iron and Steel Engineers, Pittsburgh, PA, 1985.
48. R.T.C. Choo and J. Szekely: *Weld J.*, 1994, vol. 73, pp. 25s-31s.
49. K. Hong, D.C. Weckman, and A.B. Strong: *in Trends in Welding Research*, H.B. Smartt, J.A. Johnson, and S.A. David, eds., ASM INTERNATIONAL, Materials Park, OH, 1996, pp. 399-404.
50. M. Malinowski-Brodnicka, G. den Ouden, and W.J.P. Vink: *Weld J.*, 1990, vol. 69, pp. 52s-59s.
51. K. Mundra, T. DebRoy, T. Zacharia, and S.A. David: *Weld. J.*, 1992, vol. 71, pp. 313s-20s.
52. M.H. Davies: Ph.D. Thesis, THe University of Adelaide, Adelaide, South Australia, 1995.
53. W. Pitscheneder, M. Gruböck, K. Mundra, T. DebRoy, and R. Ebner: in *Mathematical Modelling of Weld Phenomena 3*, H. Cerjak, ed., The Institute of Materials, London, 1997, pp. 41-63.
54. B.E. Launder and B.D. Spalding: *Mathematical Models of Turbulence*, Academic Press, New York, NY, 1972.
55. W.H. Giedt, L.N. Tallerico, and P.W. Fuerschbach: *Weld. J.*, 1989, vol. 68 (1), pp. 28-s-32-s.
56. M. Uda and S. Ohno: *Trans. Nat. Res. Inst. Met.*, 1973, vol. 15 (1), pp. 20-28.
57. R.T.C. Choo, J. Szekely, and R.C. Westhoff: *Metall. Trans. B*, 1992, vol. 23B, pp. 357-69.
58. J.F. Key, J.W. Chan, and M.E. McIlwain: *Weld. J.*, 1983, vol. 62 (7), pp. 179s-184s.
59. A.E.F. Gick, M.B.C. Quigley, and P.H. Richards: *J. Phys. D: Appl. Phys.*, 1973, vol. 6, pp. 1941-49.
60. J. Wendelstorf, I. Decker, H. Wohlfahrt, and G. Simon: in *Mathematical Modelling of Weld Phenomena 3*, H. Cerjak, ed., The Institute of Materials, London, 1997, pp. 848-97.
61. G.N. Haddad and A.J.D. Farmer: *Weld. J.*, 1985, vol. 64 (12), pp. 399s-342s.
62. A.J.D. Farmer and G.N. Haddad: *J. Phys. D: Appl. Phys.*, 1984, vol. 17, pp. 1189-96.
63. M.B.C. Quigley, P.H. Richards, D.T. Swift-Hook, and A.E.F. Gick: *J. Phys. D: Appl. Phys.*, 1973, vol. 6, pp. 2250-58.
64. H.A. Dinulescu and E. Pfender: *J. Appl. Phys.*, 1980, vol. 51 (6), pp. 3149-57.
65. W. Pitscheneder, R. Ebner, T. Hong, T. DebRoy, K. Mundra, and R. Benes: in *Mathematical Modelling of Weld Phenomena 4*, H. Cerjak, ed., The Institute of Materials, London, 1998, pp. 3-25.
66. C. Bodsworth: *Physical Chemistry of Iron and Steel Manufacture*, Longmans, London, 1963.
67. R.G. Ward: *An Introduction to the Physical Chemistry of Iron & Steel Making*, Edward Arnold Publishers, London, 1962.